Article

A Photocycle for Hydrogen Production from Two-Electron Mixed-Valence Complexes

Arthur J. Esswein, Adam S. Veige, and Daniel G. Nocera

J. Am. Chem. Soc., **2005**, 127 (47), 16641-16651• DOI: 10.1021/ja054371x • Publication Date (Web): 04 November 2005

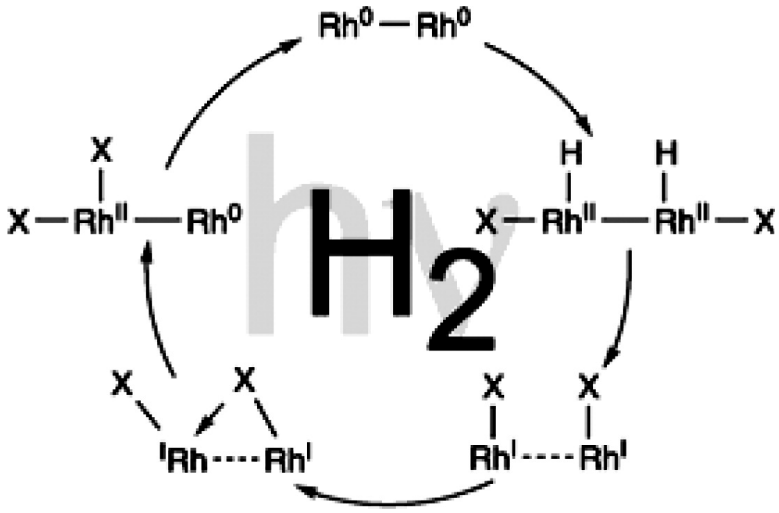

More About This Article

Additional resources and features associated with this article are available within the HTML version:

- Supporting Information
- Links to the 15 articles that cite this article, as of the time of this article download
- Access to high resolution figures
- Links to articles and content related to this article
- Copyright permission to reproduce figures and/or text from this article

View the Full Text HTML

J|A|C|S
ARTICLES
Published on Web 11/04/2005

A Photocycle for Hydrogen Production from Two-Electron Mixed-Valence Complexes

Arthur J. Esswein, Adam S. Veige,‡ and Daniel G. Nocera*

Contribution from the Department of Chemistry, 6-335, Massachusetts Institute of Technology, 77 Massachusetts Avenue, Cambridge, Massachusetts 02139-4307

Received July 1, 2005; E-mail: nocera@mit.edu

Abstract: Dihydrides of the formula $Rh_2^{II,II}(tfepma)_3H_2Cl_2$ (tfepma = (bis[bis(trifluoroethoxy)phosphino]methylamine, $MeN(P[OCH_2CF_3]_2)_2$), have been prepared by the addition of H_2 to the two-electron mixed-valence complex, $Rh_2^{0,II}(tfepma)_3Cl_2$ (**1**). Three isomeric forms with hydrides in *syn* (**2**), *anti* (**3**), and *cis* (**4**) conformations have been characterized by X-ray diffraction. Photolysis of **2** results in prompt formation of a short-lived blue photoproduct (λ_{max} = 600 nm) and a stoichiometric quantity of H_2, as determined by Toepler pump and isotopic labeling experiments. The blue photoproduct was identified as a $Rh_2^{I,I}$ complex resulting from the reductive elimination of H_2, as determined from the examination of bimetallic cores coordinated by tfepm (tfepm = (bis[bis(trifluoroethoxy)phosphino]methane, $CH_2(P[OCH_2CF_3]_2)_2$), for which complexes of the formula $M_2^{I,I}(tfepm)_3Cl_2$ (**5**, M = Rh and **6**, M = Ir) have been isolated. The $d^8\cdots d^8$ dimer of **5** converts to $Rh_2^{0,II}(tfepm)_3Cl_2CN^tBu$ (**8**) upon the addition of 1 equiv of *tert*-butylisonitrile, a result of halogen migration and disproportionation of the valence symmetric core of **5**, which is structurally compared to its two-electron mixed-valence analogue, $Rh_2^{0,II}(dfpma)_3Cl_2CN^tBu$ (**9**) (dfpma = bis(difluorophosphino)-methylamine, $MeN(PF_2)_2$). The halogen migration is captured in $Ir_2^{I,I}(tfepm)_3(\mu\text{-Cl})Cl$ (**7**), which is distinguished by the presence of a chloride that bridges the diiridium centers. Taken together, complexes **1**−**9** permit the construction of a complete photocycle for the photogeneration of H_2 by dirhodium dfpma complexes in homogeneous solutions of hydrohalic acids.

Introduction

A great technological challenge facing our global future is the development of renewable energy. Rising standards of living in a growing world population will cause global energy consumption to increase dramatically over the next half century. Energy consumption is predicted to increase at least 2-fold, from our current burn rate of 12.8 to 28−35 TW by 2050.[1,2] A short-term response to this challenge is the use of methane and other petroleum-based fuels as hydrogen sources.[3] However, external factors of economy, environment, and security dictate that this energy need be met by renewable and sustainable sources,[3−9] with water emerging prominently as the primary carbon-neutral hydrogen source and light as an energy input.

Our group has had recent success in using two-electron mixed-valence (M^n-M^{n+2}) cores to manage the two-electron chemistry of hydrogen production and activation. Two-electron mixed-valence hydrido−halides of diiridium undergo efficient H_2 elimination.[10−12] This H_2 reactivity is derived from intermetal cooperativity engendered by ancillary diphosphazane ligands, which are able to accommodate the electronic and coordination asymmetry of the adjacent metals as a hydrogen atom is shuttled between them.[12,13] For the case of dirhodium complexes, H_2 production upon HX addition to a $Rh_2^{0,0}$ center is photopromoted and yields a two-electron mixed-valence $Rh^0-Rh^{II}X_2$ complex as the photoproduct; the $Rh^{II}-X$ bond may be photoactivated in the presence of a halogen trap,[14,15] thus allowing us to establish a photocycle for H_2 production from homogeneous

‡ Current address: Department of Chemistry, University of Florida, P.O. Box 117200, Gainesville, FL 32611-7200.

(1) Hoffert, M. I.; Caldeira, K.; Jain, A. K.; Haites, E. F.; Harvey, L. D. D.; Potter, S. D.; Schlesinger, M. E.; Schneider, S. H.; Watts, R. G.; Wigley T. M. L.; Wuebbles, D. J. *Nature* **1998**, *395*, 881−884.
(2) Lewis, N. S. *Energy and Transportation*; The National Academies Press: Washington, DC, 2003; pp 33−39.
(3) *Basic Research Needs for the Hydrogen Economy*; A Report from the Basic Energy Sciences Workshop on Hydrogen Production, Storage, and Use; U.S. Department of Energy: Washington, DC, 2003.
(4) *World Energy Assessment Report: Energy and the Challenge of Sustainability*; United Nations Development Program; United Nations: New York, 2003.
(5) *Basic Research Needs to Assure a Secure Energy Future*; A Report from the Basic Energy Sciences Advisory Committee; U.S. Department of Energy: Washington, DC, 2003.
(6) *Energy and National Security*; Karas, T. H.; Sandia Report SAND2003-3287, 2003.
(7) Address to the National Hydrogen Association, Secretary of Energy Spencer Abraham, 5 March 2003; available at http://www.energy.gov/engine/content.do?PUBLIC_ID=13384&BT_CODE=PR_SPEECHES&TT_CODE=PRESSRELEASE.
(8) *The Effect on the National Security of Imports of Crude Oil and Refined Petroleum Products*; U.S. Department of Commerce, An Investigation Conducted Under Section 232 of the Trade Expansion Act of 1962, as Amended, November 1999; p ES-9.
(9) Goodstein, D. *Out of Gas: The End of the Age of Oil*; Norton: New York, 2004.
(10) Heyduk, A. F.; Nocera, D. G. *Chem. Commun.* **1999**, 1519−1520.
(11) Heyduk, A. F.; Nocera, D. G. *J. Am. Chem. Soc.* **2000**, *122*, 9415−9426.
(12) Gray, T. G.; Veige, A. S.; Nocera, D. G. *J. Am. Chem. Soc.* **2004**, *126*, 9760−9678.
(13) Veige, A. S.; Gray, T. G.; Nocera, D. G. *Inorg. Chem.* **2005**, *44*, 17−26.
(14) Heyduk, A. F.; Macintosh, A. M.; Nocera, D. G. *J. Am. Chem. Soc.* **1999**, *121*, 5023−5032.
(15) Odom, A. L.; Heyduk, A. F.; Nocera, D. G. *Inorg. Chim. Acta* **2000**, *297*, 330−337.

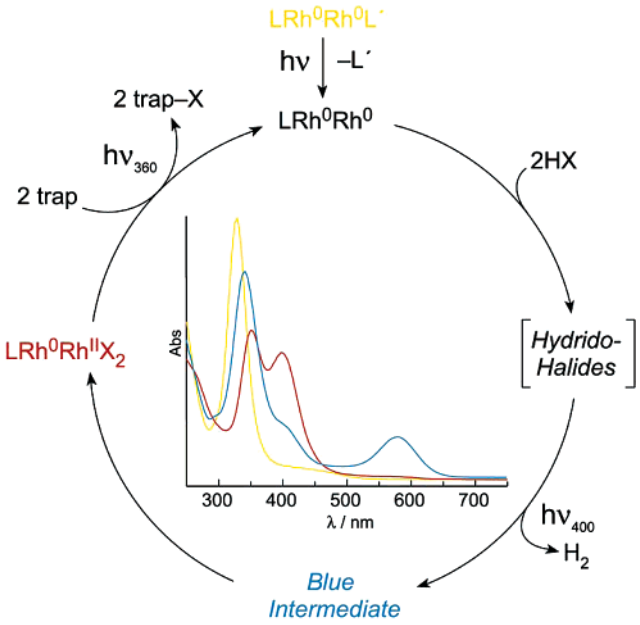

Figure 1. Photocycle for H_2 production by $Rh_2^{0,0}$ dfpma in HX solutions. Observed photoproducts of the cycle are indicated with their accompanying color-coded absorption spectra.

Chart 1

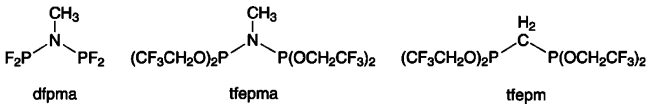

HX (X = Cl, Br) solutions.[16] As depicted in Figure 1, a photon removes an axial CO from the $Rh_2^{0,0}$ complex, opening a coordination site for HX attack (the axial site may also be opened thermally). Disappearance of the $Rh_2^{0,0}$ complex is accompanied by the formation of 1 equiv of H_2 and the appearance of a blue intermediate, which quickly converts to the $Rh^0-Rh^{II}X_2$ complex from which the coordinatively unsaturated $Rh_2^{0,0}$ complex is regenerated by $Rh^{II}-X$ bond photoactivation. In this phototransformation, H_2 elimination is facile, and neither hydride− nor hydrido−halide intermediates are observed.

Whereas Figure 1 establishes a photocycle, the process by which H_2 photogeneration occurs is heretofore unknown. The following issues remain unresolved: (1) What is the nature of the initial hydrogen−halide addition product? (2) What is the nature of the blue photointermediate, and what is the photoreaction that leads to its production? (3) How does the blue intermediate convert to the $Rh^0-Rh^{II}X_2$ complex, thereby allowing the photocycle to be closed? (4) What is the step in the photocycle that limits the overall H_2 production efficiency?

We now address these outstanding issues by tuning the electronic properties of the ligand. Specifically, the two-electron mixed valency required for the photocycle of Figure 1 is enforced by the three $MeN(PF_2)_2$ (dfpma = bis[difluorophosphino]methylamine) bidentate diphosphazane ligands (Chart 1) that span the bimetallic core.[17] In the dfpma architecture, π-accepting fluorophosphine groups are adjacent to the lone pair of an amine bridgehead, giving rise to an acceptor−donor−acceptor (A−D−A) electronic motif. Because the phosphine groups may π-accept electrons from the metal or from the lone pair of nitrogen, the ligand is able to concomitantly accommodate metals both in low and moderate oxidation states. By tuning the electronic accepting properties of the ligand from $-PF_2$ to the slightly less π-accepting and more bulky $-P(OCH_2CF_3)_2$ of $MeN[P(OCH_2CF_3)_2]_2$ (tfepma = bis[bis(trifluoroethoxy)phosphino]methylamine)[18] and the amine donor bridgehead to the methylene group of $H_2C[P(OCH_2CF_3)_2]_2$ (tfepm = bis[bis(trifluoroethoxy)phosphino]methane) (Chart 1), we are able to reveal the nature of all intermediates relevant to the photocycle. In doing so, we are able to examine independently each step of the photocycle and ascertain the factors controlling the photoefficiency for H_2 production.

Experimental Section

General Considerations. All manipulations were carried out in an N_2-filled glovebox or under an inert atmosphere provided by a Schlenk line unless otherwise noted. All solvents were reagent grade (Aldrich) or better and were dried and degassed by standard methods.[19] $MeN(P[OCH_2CF_3]_2)_2$ (tfepma),[20,21] $CH_2(P[OCH_2CF_3]_2)_2$ (tfepm),[22,23] and $MeN(PF_2)_2$ (dfpma)[24] were prepared by literature methods. $[Rh^I(COD)Cl]_2$ and $[Ir^I(COD)Cl]_2$ (COD = cyclooctadiene) (Strem), H_2, D_2 (BOC gases), HCl, and *tert*-butylisonitrile (Aldrich) were used as received.

Methods. NMR data were collected at the MIT Department of Chemistry Instrument Facility (DCIF) on a Varian Inova Unity 500 spectrometer. NMR solvents (CD_2Cl_2, CD_3CN, THF-d_8, toluene-d_8) were purchased from Cambridge Isotope Labs and purified by standard procedures prior to use. ^1H NMR spectra (500 MHz) were referenced to the residual proteo impurities of the given solvent. ^2H NMR spectra (76.5 MHz) were recorded in proteo solvents and referenced to natural abundance deuterium of the solvent. $^{31}P\{^1H\}$ NMR (202.5 MHz) spectra were referenced to an external 85% H_3PO_4 standard. All chemical shifts are reported in the standard δ notation in parts per million; positive chemical shifts are to higher frequency from the given reference. Elemental analyses were performed by Robertson Microlit Laboratories, Madison, NJ. Photolysis experiments were conducted using a 1000 W Xe/Hg lamp in an Oriel model 66021 lamp housing. Wavelength selection of the excitation light was accomplished by employing appropriate glass filters. Photolysis experiments were conducted in 1 cm quartz cells isolated from the ambient atmosphere by two Teflon valves. NMR photolysis experiments were conducted in quartz J. Young NMR tubes. Solutions were freeze−pump−thawed for three cycles (1×10^{-5} Torr) prior to photolysis. UV−vis spectra were recorded on a Spectral Instruments 400 series diode array spectrometer and referenced against the appropriate solvent. The Toepler pump was calibrated by introducing a known pressure of hydrogen into a gas bulb of known volume and burning over hot CuO.

Preparation of $Rh_2^{0,II}(tfepma)_3Cl_2$ (1). To a saturated CH_2Cl_2 solution of $[Rh^I(COD)Cl]_2$ (778 mg, 1.58 mmol) was added tfepma (2.305 g, 4.73 mmol, 3 equiv) dropwise to effect an immediate color change from dark orange to green. The solution was allowed to stir overnight, the green precipitate allowed to settle, and the supernatant removed. The solid was collected on a frit, washed with CH_2Cl_2 (5 mL) and pentane (4 × 5 mL), and dried under vacuum to yield 2.279

(16) Heyduk, A. F.; Nocera, D. G. *Science* **2001**, *293*, 1639−1641.
(17) Gray, T. G.; Nocera, D. G. *Chem. Commun.* **2005**, 1540−1542.
(18) Tolman, C. A. *Chem. Rev.* **1977**, *77*, 313−348.
(19) Armarego, W. L. F.; Perrin, D. D. *Purification of Laboratory Chemicals*, 4th ed.; Butterworth-Heinmann: Oxford, 1996.
(20) Ganesan, M.; Krishnamurthy, S. S.; Nethaji, M. *J. Organomet. Chem.* **1998**, *570*, 247−254.
(21) Balakrishna, M. S.; Prakasha, T. K.; Krishnamurthy, S. S.; Siriwardane, U.; Hosmane, N. S. *J. Organomet. Chem.* **1990**, *390*, 203−216.
(22) Hietkamp, S.; Sommer, H.; Stelzer, O. *Inorg. Synth.* **1989**, *27*, 120−121.
(23) Bitterwolf, T. E.; Raaghuveer, K. S. *Inorg. Chim. Acta* **1990**, *172*, 59−64.
(24) Nixon, J. F. *J. Chem. Soc. A* **1968**, 2689−2692.

g (83%) of **1** as a green powder. Broadened NMR resonances are symptomatic of the dynamic solution behavior of **1** in polar solvents.[11] ^{1}H NMR (THF-d_8): δ 2.74 ppm (bs, 3H), 2.96 ppm (bs, 6H), 4.54 ppm (m, 8H), 4.68−5.07 ppm (m, 16H). ^{31}P{^{1}H} NMR (THF-d_8): δ 101 ppm (b, 1P), 126−135 ppm (m, 5P). Anal. Calcd for $C_{27}H_{33}N_3Cl_2F_{36}O_{12}P_6Rh_2$: C, 18.69; H, 1.91; N, 2.42. Found: C, 18.69; H, 1.68; N, 2.34. Crystals suitable for X-ray diffraction were grown from CH_2Cl_2/pentane solution as green shards.

Preparation of $Rh_2^{II,II}$(tfepma)$_3H_2Cl_2$ (2−4). In a thick-walled 200 mL glass bomb, 1.995 g (1.15 mmol) of **1** was dissolved in 15 mL of THF. The bomb was attached to a high vacuum line, the solution was freeze−pump−thawed (three cycles), and 1 atm of H_2 was added. The solution was thawed and allowed to stir in the dark for 1 week, during which time the solution had turned from green/brown to dark red. The solvent was removed in vacuo, and the resulting sticky solid was washed with pentane (5 × 5 mL) and finally CH_2Cl_2 (5 mL) to give a yellow solid. The solid was recrystallized twice from a minimum of hot CH_2Cl_2 to give 0.574 g (29%) of **2** as a yellow crystalline solid. NMR spectra of the crystalline material dissolved in THF-d_8 reveals multiple products with **2** as the 95% constituent. ^{1}H NMR (THF-d_8): δ −9.77 ppm (m, 2H), 2.89 ppm (t, 3.4 Hz, 6H), 3.06 ppm (t, 6.1 Hz, 3H), 4.48−4.82 ppm (m, 24 H). ^{31}P{^{1}H} NMR (THF-d_8): δ 131.40 ppm (bs, 2P), 136.77 (bd, 131.0 Hz, 4P). Anal. Calcd for $C_{27}H_{35}N_3Cl_2F_{36}O_{12}P_6Rh_2$: C, 18.64; H, 2.03; N, 2.41. Found: C, 18.63; H, 1.95; N, 2.56. Yellow block crystals suitable for X-ray diffraction were obtained from repeated recrystallizations of solid from hot CH_2Cl_2 solutions. Deuterated material (**2**-d_2) was synthesized by the addition of deuterium to 2.030 g of **1** in an analogous procedure and workup to give 0.732 g (35%) of **2**-d_2 after two recrystallizations from CH_2Cl_2. ^{1}H NMR (THF-d_8): δ 2.89 ppm (t, 3.4 Hz, 6H), 3.06 ppm (t, 6.1 Hz, 3H), 4.48−4.82 ppm (m, 24 H). ^{2}H NMR (THF): δ −10.3 ppm (m). ^{31}P{^{1}H} NMR (THF-d_8): δ 134.20 ppm (bs, 2P), 139.55 (bd, 134.3 Hz, 4P). Anal. Calcd for $C_{27}H_{33}D_2N_3Cl_2F_{36}O_{12}P_6Rh_2$: C, 18.61; H, 2.14; N, 2.41. Found: C, 18.60; H, 2.04; N, 2.36.

Undisturbed CH_3CN solutions of **2** promote the deposition of **3** as crystalline yellow blocks suitable for X-ray diffraction. The asymmetric unit contained half the molecule with the remaining portion generated by a crystallographic C_2 axis. Dissolution of these crystals in THF-d_8 revealed multiple products by ^{1}H NMR, the major product of which has N−Me resonances at 3.03 and 2.78 ppm integrating in a 2:1 ratio. Multiple overlapping hydride resonances precluded assignment. After standing for long periods (>1 week), CH_2Cl_2/pentane solutions collected from the isolation of **2** afforded yellow/green blocks of **4** suitable for X-ray diffraction. Dissolution of the yellow/green single crystals of **4** in THF-d_8 initially gives a light green solution that rapidly changes to yellow. Multiple components are observed in the ^{1}H NMR, with N−Me resonances at 2.78, 2.86, and 2.97 (a shoulder at 3.03 ppm accords with a resonance of **3**). Consistent with the dynamic behavior of **2**, solutions of the compound maintained in the dark show the growth of the N−Me resonances diagnostic of **3** and **4** at the expense of N−Me resonances of **2** at 2.89 and 3.06 ppm.

Preparation of $Rh_2^{I,I}$(tfepm)$_3Cl_2$ (5). To a minimum amount of CH_2Cl_2 was added 731 mg (1.48 mmol) of [Rh^I(COD)Cl]$_2$ to afford an orange solution; 2.1 g (4.45 mmol, 3 equiv) of tfepm was then added dropwise, immediately effecting a color change to dark purple. The solution was stirred for 12 h after which a microcrystalline precipitate was allowed to settle. The purple supernatant was removed, and the solid was washed repeatedly with pentane until the washings showed no discernible color. Residual solvent was removed in vacuo, giving 2.07 g (82%) of **5** as a purple solid. ^{1}H NMR (CD_2Cl_2): δ 3.04 ppm (q, 13.4 Hz, 2H), 3.32 ppm (t, 12.2 Hz, 2H), 3.51 ppm (dt, 12.5 Hz, 9.8 Hz, 2H), 3.97 ppm (q, 9.2 Hz, 2H), 4.2−4.7 ppm (m, 22H). ^{31}P-{^{1}H} NMR (CD_2Cl_2): δ 158.03 ppm (dm, 625.8 Hz, 2P), 165.64 ppm (m, 2P), 171.28 ppm (dm, 625.8 Hz, 2P). Anal. Calcd for $C_{27}H_{30}Cl_2F_{36}O_{12}P_6Rh_2$: C, 19.15; H, 1.79. Found: C, 19.10; H, 1.35. λ_{max}/nm (ϵ/M^{-1} cm^{-1}) in toluene: 293 (4800); 376 (2400); 507 (9300). Crystals suitable for X-ray diffraction were grown from CH_2Cl_2/pentane solution as dark pink blocks.

Preparation of $Ir_2^{I,I}$(tfepm)$_3Cl_2$ (6). To a stirred suspension of [Ir^I(COD)Cl]$_2$ (141 mg, 0.210 mmol) in 10 mL of toluene was added dropwise 297 mg (3.0 equiv) of tfepm, immediately causing a color change from light orange to dark brown/red. The solution was allowed to stir for 3 days during which the solution color turned to dark purple. The solution was placed in a freezer (−40 °C) overnight, filtered, concentrated to a volume of 5 mL, and then recrystallized with pentane. The resulting solid was then washed with pentane (3 × 5 mL) giving 114 mg (29%) of **6** as a purple solid. ^{1}H NMR (toluene-d_8): δ 2.77 ppm (q, 14.5 Hz, 2H), 2.84 ppm (t, 13.1 Hz, 2H), 3.09 ppm (dt, 12.5 Hz, 11.9 Hz, 2H), 3.63 ppm (quint, 9.2 Hz, 2H), 3.83 ppm (m, 4H), 4.1−4.7 ppm (m, 18H). ^{31}P{^{1}H} NMR (toluene-d_8): δ 116.61 ppm (m, 2P), 142.29 ppm (dm, 623.8 Hz, 2P), 155.15 ppm (dm, 623.8 Hz, 2P). Anal. Calcd for $C_{27}H_{30}Cl_2F_{36}O_{12}P_6Ir_2$: C, 17.33; H, 1.61. Found: C, 17.61; H, 1.69. λ_{max}/nm (ϵ/M^{-1} cm^{-1}) in toluene: 313 (5800); 352 (3800); 571 (7100). Crystals suitable for X-ray diffraction were grown from slowly evaporated toluene solutions as purple blocks. The asymmetric unit contained two crystallographically and chemically distinct molecules (**6** and **7**) and five and a half toluene molecules. Two toluenes were disordered over two positions, and the half toluene was disordered over a crystallographic inversion center. Crystals of **6** and **7** isolated from each other could be obtained from slowly evaporating benzene solutions. **6** grew as purple blocks; the asymmetric unit contained half the molecule and two benzene molecules as solvents of crystallization (see Supporting Information). **7** grew as yellow shards from the purple benzene solutions of **6**. The asymmetric unit contained two molecules of benzene as solvents of crystallization (see Supporting Information). Attempts to synthesize **7** directly have so far proven unsuccessful, obviating a full NMR characterization.

Preparation of $Rh_2^{0,II}$(tfepm)$_3Cl_2CN^tBu$ (8). To a stirred solution of $Rh_2^{I,I}$(tfepm)$_3Cl_2$ (**5**) (500 mg, 0.295 mmol) in CH_2Cl_2 was added 25 mg (0.301 mmol, 1 equiv) of *tert*-butylisonitrile, causing an immediate color change from purple to dark red. The reaction was allowed to stir for 3 h, and then solvent was removed. The resulting orange solid was washed with pentane to yield 520 mg (99%) of **7**. ^{1}H NMR (CD_3CN): δ 1.40 ppm (s, 9H), 3.63 ppm (bd, 11.6 Hz, 2H), 3.79 ppm (dd, 7.6 Hz, 6.7 Hz, 2H), 4.27−4.67 ppm (m, 20H), 4.88 ppm (d, 14.0 Hz, 2H), 5.02 ppm (m, 4H). ^{31}P{^{1}H} NMR (CD_3CN): δ 157.68 ppm (m, 1P), 159.55 ppm (m, 2P), 168.82 ppm (ov m, 3P). Anal. Calcd for $C_{32}H_{39}Cl_2F_{36}NO_{12}P_6Rh_2$: C, 21.64; H, 2.21; N, 0.79. Found: C, 21.62; H, 2.19; N, 0.73. λ_{max}/nm (ϵ/M^{-1} cm^{-1}) in Et_2O: 342 (11600); 389 (7000); 498 (2500). Crystals suitable for X-ray diffraction were grown from CH_2Cl_2/pentane solution as red blocks. The asymmetric unit contained two crystallographically distinct but chemically equivalent molecules and a molecule each of pentane and CH_2Cl_2 as solvents of crystallization.

Preparation of $Rh_2^{0,II}$(dfpma)$_3$ Cl_2CN^tBu (9). To a stirred solution of [Rh^I(COD)Cl]$_2$ (272 mg, 0.551 mmol) in 10 mL of CH_2Cl_2 was added 46 mg (0.551 mmol, 1 equiv) of *tert*-butylisonitrile. Dropwise addition of 276 mg (1.655 mmol, 3 equiv) of dfpma dissolved in 2 mL of CH_2Cl_2 affected an immediate color change to dark red. The solution was allowed to stir for 3 h and the solvent stripped. The resulting solid was then suspended in Et_2O, filtered, washed with Et_2O (4 × 5 mL), and then washed off the filter with CH_2Cl_2. The solvent was stripped to give 167 mg (35%) of **9** as an orange solid. ^{1}H NMR (CD_3CN): δ 1.52 ppm (s, 9H), 2.99 ppm (bt, 3H), 3.06 (bs, 6H). Anal. Calcd for $C_8H_{18}Cl_2F_{12}N_4P_6Rh_2$: C, 11.16; H, 2.11; N, 6.51 Found: C, 11.40; H, 1.88; N, 6.35. Crystals suitable for X-ray diffraction were grown from CH_2Cl_2/pentane solution as orange blocks.

X-ray Crystallographic Details. Single crystals were immersed in a drop of Paratone N oil on a clean microscope slide, affixed to either a glass fiber or a human hair coated in epoxy resin and then cooled to either −80, −123, or −173 °C. The crystals were then mounted on either a Siemens three circle goniometer platform equipped with a CCD

detector or with an APEX detector. A graphite monochromator was employed for wavelength selection of the Mo K_α radiation ($\lambda = 0.71073$ Å). The data were processed and refined using the program SAINT supplied by Siemens Industrial Automation Inc. Structures were solved by a Patterson heavy atom map and refined by standard difference Fourier techniques in the SHELXTL program suite (6.10 v., Sheldrick G. M., and Siemens Industrial Automation Inc., 2000). Disordered atoms in solvent and $-OCH_2CF_3$ groups were fixed at idealized bond lengths, and occupancies were refined isotropically. Hydrogen atoms were placed in calculated positions using the standard riding model and refined isotropically; all other atoms were refined anisotropically. Unit cell parameters, morphology, and solution statistics for complexes **1**−**9** are summarized in Table 1. All thermal ellipsoid plots are drawn at the 50% probability level, with hydrogens, $-CH_2CF_3$ groups, N−Me groups, and solvents of crystallization omitted for clarity. Selected bond distances and bond angles are listed in Tables 2−4 (for compounds **1**−**7**) and Table S11 (for compounds **8** and **9**) in Supporting Information.

Computational Details. The Gaussian 98 program suite was employed for computational studies.[25] Geometry optimizations were initiated using atomic coordinates obtained from X-ray diffraction data. Trifluoroethoxy groups on the tfepma and tfepm ligands were replaced with fluorines. Hydrides not located crystallographically were placed at idealized positions with an M−H bond length of 1.600 Å. DFT calculations were carried out using the exchange functional of Becke[26] in conjunction with the P86 correlation functional of Perdew.[27] Relativistic core potentials were used for rhodium along with the standard Hay−Wadt double-ζ basis set,[28] augmented by the optimized Rh 5p function of Couty and Hall.[29] The 6-31G(d,p) basis of Pople and co-workers[30,31] was applied to all other atoms. Optimized geometries were confirmed as energy minima by analytical frequency calculations. Reported energies are the sum of electronic and thermal free energies and are corrected for zero point energies. The calculations reported here are for molecules in the gas phase, and no attempt has been made to correct for the effects of solvation.

Results

Structural and Thermal Reaction Chemistry. Two-electron mixed-valence species **1** is the keystone for the dihydride/hydrogen chemistry of pertinence to the photocycle shown in Figure 1. The complex, whose crystal structure is shown in Figure 2, is distinguished by the disposition of the three A−D−A ligands about the bimetallic core. As summarized in Chart 2 (only the PNP backbones of the ligands are depicted), the sterically less-encumbering dfpma ligand exhibits a preference to bridge $Rh_2^{0,II}$ centers. In contrast, one tfepma ligand in **1** chelates the Rh^0 center to afford a trigonal bipyramidal coordination sphere, which is defined by the average $\angle(P-Rh-P)_{avg} = 120°$ in the trigonal plane and a nearly linear $P_{ax}-Rh^0-Rh^{II}$ axis (see Table 2). Computational and synthetic studies suggest that bulky substituents on the phosphorus atoms, such as the trifluoroethoxy groups of tfepma, increases the chelating power of the ligand.[32,33] The absence of a third phosphorus ligand in the equatorial plane of Rh^{II} demands the

Table 1. Crystallographic Summary for Complexes **1**−**9**

	1·0.25(CH_2Cl_2)	**2**	**3**·CH_3CN	**4**	**5**	**6**·**7**·2.75($C_6H_5CH_3$)	**8**·CH_2Cl_2·C_5H_{12}	**9**
formula	$C_{27}H_{33}N_3Cl_2F_{36}O_{12}P_6Rh_2$	$C_{27}H_{35}N_3Cl_2F_{36}O_{12}P_6Rh_2$	$C_{27}H_{35}N_3Cl_2F_{36}O_{12}P_6Rh_2$	$C_{27}H_{35}N_3Cl_2F_{36}O_{12}P_6Rh_2$	$C_{27}H_{30}Cl_2F_{36}O_{12}P_6Rh_2$	$C_{27}H_{30}Cl_2F_{36}O_{12}P_6Ir_2$	$C_{32}H_{38}Cl_2F_{36}NO_{12}P_6Rh_2$	$C_8H_{18}Cl_2F_{12}N_4P_6Rh_2$
fw, g/mol	1760.84	1740.12	1781.17	1740.12	1693.05	2125.00	1854.72	860.80
cryst. syst.	monoclinic	monoclinic	monoclinic	triclinic	tetragonal	triclinic	triclinic	monoclinic
space group	*C*2/*c*	$P2_1/n$	*C*2/*c*	*P*$\bar{1}$	*I*$\bar{4}$2*d*	*P*$\bar{1}$	*P*$\bar{1}$	$P2_1/n$
color	green	yellow	yellow	green	purple	purple	orange	orange
a (Å)	22.716(9)	13.0479(11)	22.496(4)	11.5832(10)	23.8123(8)	12.2242(12)	16.226(2)	22.716(9)
b (Å)	12.743(9)	17.4813(14)	13.547(2)	12.5020(11)	23.8123(8)	21.880(2)	19.218(3)	12.743(9)
c (Å)	39.700(15)	25.268(2)	21.382(4)	21.6206(19)	20.0571(13)	27.148(3)	24.237(3)	39.700(15)
α (°)	90	90	90	98.106(2)	90	91.330(2)	110.279(3)	90
β (°)	92.475(14)	100.247(2)	91.910(4)	93.609(2)	90	102.312(2)	94.226(3)	92.084(2)
γ (°)	90	90	90	109.725(2)	90	90.810(2)	104.932(3)	90
V (Å^3)	11482(10)	5671.6(8)	6513(2)	2897.2(4)	11372.89(9)	7090.9(12)	6738.3(16)	2581.6(6)
Z	8	4	4	2	8	4	4	4
T (°C)	−123 (2)	−80 (2)	−80 (2)	−80 (2)	−173 (2)	−173 (2)	−173 (2)	−80(2)
no.data	12542	5994	4407	8314	7053	24076	19061	6376
res.	34	0	0	17	0	24	32	0
param.	786	792	432	814	385	1820	1693	313
$R1^a$	0.0664	0.0712	0.0613	0.0585	0.0274	0.0392	0.0734	0.0363
$wR2^a$	0.1620	0.1718	0.1397	0.1239	0.0715	0.0953	0.1954	0.0932
GOF^b	1.042	1.139	1.033	1.068	1.058	1.048	1.041	1.148

^{a} $R1 = \sum||F_o| - |Fc||/\sum|F_o|$; $wR2 = [\sum w(F_o^2 - F_c^2)^2/\sum wF_o^4]^{1/2}$. Refinement on F_o^2 for all reflections (having $F_o^2 \geq -3\sigma(F_o^2)$). *w*R2 and GOF based on F_o^2, *R*1 based on F_o, with F_o set to zero for negative F_o^2. The observed criterion of $F_o^2 > 2\sigma(F_o^2)$ is used only for calculating *R*1 and is not relevant to the choice of reflections for refinement. ^{b} GOF = $[\sum w(F_o^2 - F_c^2)^2/(n-p)]^{1/2}$ (n = number of data, p = number of parameters varied; $w = [\sigma^2F_o^2 + (0.0638P)^2]^{-1}$, where $P = [\max(F_o^2, 0) + 2F_c^2]/3$.

(25) Frisch, M. J. et al. *Gaussian 98*, revision A.9: Gaussian, Inc.: Pittsburgh, PA, 1998.
(26) Becke, A. D. *Phys. Rev. A* **1988**, *38*, 3098−3100.
(27) Perdew, J. P. *Phys. Rev. B* **1986**, *33*, 8822−8824.
(28) Hay, P. J.; Wadt, W. R. *J. Chem. Phys.* **1985**, *82*, 270−283; 284−298; 299−310.
(29) Couty, M.; Hall, M. B. *J. Comput. Chem.* **1996**, *11*, 1359−1370.
(30) Hariharan, P. C.; Pople, J. A. *Theor. Chim. Acta* **1973**, *28*, 213−222.
(31) Francl, M. M.; Pietro, W. J.; Hehre, W. J.; Binkley, J. S.; Gordon, M. S.; DeFrees, D. J.; Pople, J. A. *J. Chem. Phys.* **1982**, *77*, 3654−3655.
(32) McKee, M. L.; Hill, W. E. *J. Phys. Chem. A* **2002**, *106*, 6201−6205.
(33) Barklay, J. V.; Ellis, M.; Higgins, S. J.; McCart, M. K. *Organometallics* **1998**, *17*, 1725−1731.

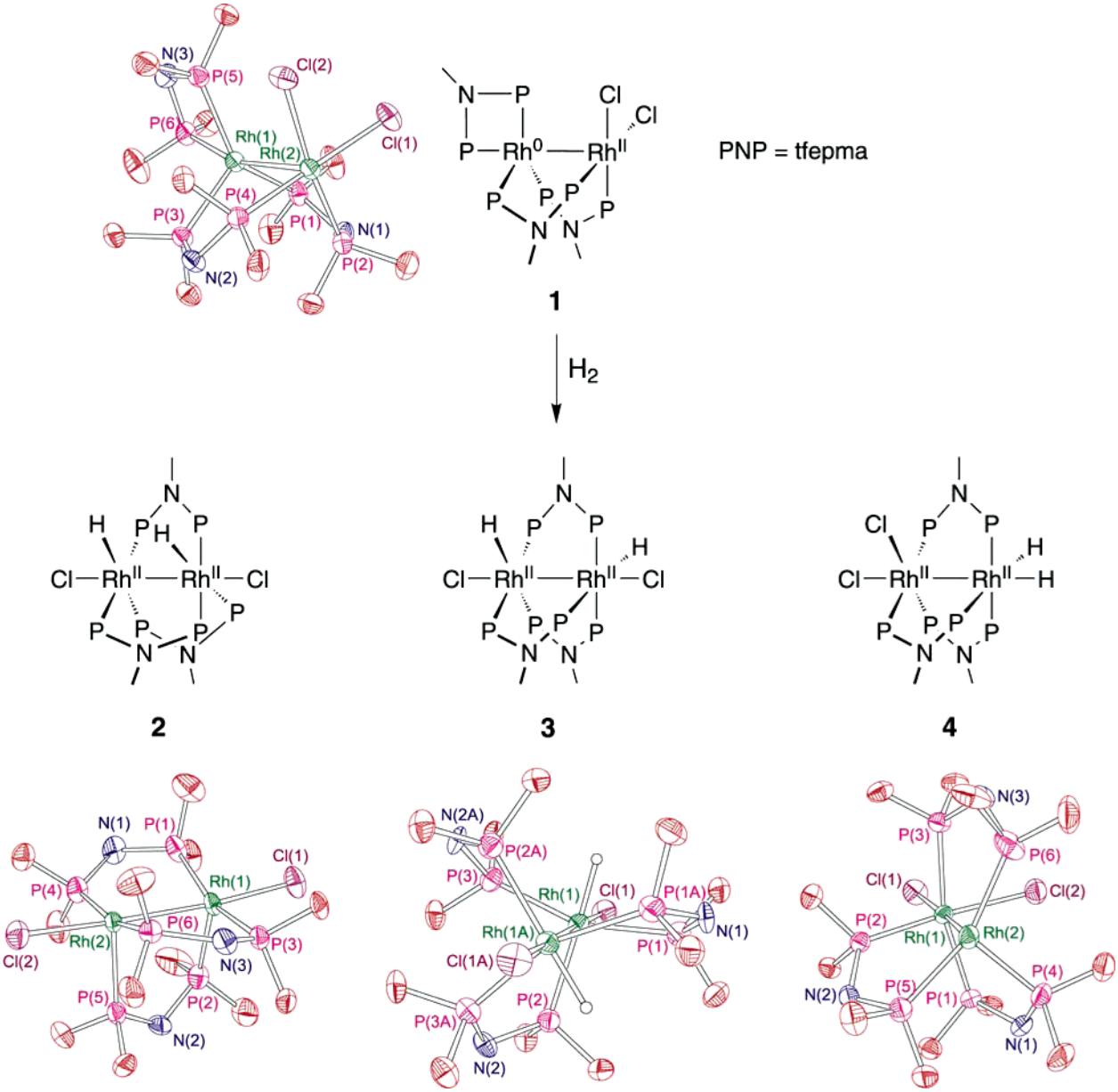

Figure 2. Hydrogenation of $Rh_2^{0,II}(tfepma)_3Cl_2$ (**1**) yields three dihydrido−dihalide isomers of $Rh_2^{II,II}(tfepma)_3H_2Cl_2$ (**2**−**4**). Thermal ellipsoids are drawn at the 50% probability level, and the N−Me and $-CH_2CF_3$ groups of the tfepma ligand have been omitted for clarity. Only atom numbers of pertinence to Table 3 are included. Full atom numbering scheme is presented in Supporting Information.

Chart 2

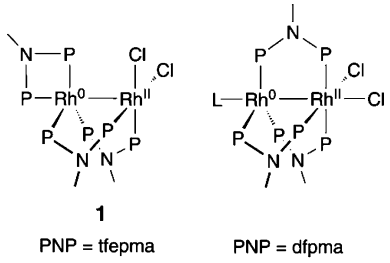

equatorial coordination of the two halides at the Rh^{II} center, leaving its axial coordination site vacant and engendering an overall square pyramidal geometry. This precise coordination motif has been observed previously for diiridium centers.[10] Indeed, **1** and its diiridium congener are structurally homologous as indicated by a comparison of the metrics listed in Table 2 for the two compounds. The most noted deviation is a slight decrease in the metal−metal bonding distance from 2.7871(8) Å in $Ir_2^{0,II}(tfepma)_3Cl_2$ to 2.7450(12) Å in **1**.

Coordinative unsaturation trans to the metal−metal axis of the $M_2^{0,II}$ core results in an extensive reaction chemistry for the structurally congruent $Ir_2^{0,II}(tfepma)_3Cl_2$ with small molecule substrates,[11,34] including hydrogen and hydrogen halides.[12,13] As exemplified by Figure 2, this chemistry is preserved for the structurally analogous dirhodium complex; hydrogen reacts with **1** to yield $Rh_2^{II,II}(tfepma)_3H_2Cl_2$ in three isomeric forms. The crystal structures of the three isomers are shown in Figure 2 and relevant bond distances and angles for the three complexes in Table 3.

Compound **2** is the predominate product, and single crystals may be isolated by repeated recrystallizations from slowly cooled CH_2Cl_2 solutions containing the mixture of isomers

(34) Veige, A. S.; Nocera, D. G. *Chem. Commun.* **2004**, *17*, 1958−1959.

Table 2. Selected Crystallographic Bond Distances (Å) and Angles (°) for the $Rh_2^{0,II}(tfepma)_3Cl_2$ (1) and Diiridium Congener $Ir_2^{0,II}(tfepma)_3Cl_2$

Bond lengths/Å

	$Rh_2^{0,II}(tfepma)_3Cl_2$	$Ir_2^{0,II}(tfepma)_3Cl_2$
M(1)−M(2)	2.7450(12)	2.7871(8)
M(2)−Cl(1)	2.364(2)	2.363(4)
M(2)−Cl(2)	2.34584(18)	2.375(4)
M(1)−P(1)	2.2395(17)	2.235(4)
M(2)−P(2)	2.1861(18)	2.190(4)
M(1)−P(3)	2.292(2)	2.269(4)
M(2)−P(4)	2.188(2)	2.189(4)
M(1)−P(5)	2.2819(17)	2.273(4)
M(1)−P(6)	2.1801(17)	2.206(4)

Bond angles/°

	$Rh_2^{0,II}(tfepma)_3Cl_2$	$Ir_2^{0,II}(tfepma)_3Cl_2$
P(1)−M(1)−P(3)	106.75(6)	106.72(16)
P(3)−M(1)−P(5)	114.90(5)	115.74(15)
P(5)−M(1)−P(1)	137.41(6)	136.82(16)
P(5)−M(1)−P(6)	69.75(6)	69.44(15)
P(6)−M(1)−M(2)	163.94(5)	163.98(12)
P(2)−M(2)−P(4)	96.04(5)	96.24(16)
Cl(1)−M(2)−P(4)	171.59(6)	169.40(15)
Cl(2)−M(2)−P(2)	173.73(5)	172.77(15)

Torsion angles/°

	$Rh_2^{0,II}(tfepma)_3Cl_2$	$Ir_2^{0,II}(tfepma)_3Cl_2$
P(1)−M(1)−M(2)−P(2)	−32.83(6)	32.42(16)
P(3)−M(1)−M(2)−P(4)	−22.51(5)	23.35(15)
Cl(1)−M(1)−M(2)−P(5)	−84.00(6)	82.46(16)
Cl(1)−M(1)−M(2)−P(5)	4.29(5)	−4.59(14)

Table 3. Selected Crystallographic Bond Distances (Å) and Angles (°) for Complexes **2**, **3**, and **4**

Bond lengths/Å

	2	**3**[a]	**4**[b]
Rh(1)−Rh(2)	2.7087(12)	2.7127(13)	2.7657(8)
Rh(1)−Cl(1)	2.451(3)	2.459(2)	2.5442(19)
Rh(2)−Cl(2)	2.446(3)	−	2.4110(19)
Rh(1)−P(1)	2.249(3)	2.255(2)	2.2643(19)
Rh(1)−P(2)	2.303(3)	2.293(2)	2.1930(19)
Rh(1)−P(3)	2.231(3)	2.244(2)	2.2892(19)
Rh(2)−P(4)	2.243(3)	−	2.284(2)
Rh(2)−P(5)	2.305(3)	−	2.217(2)
Rh(2)−P(6)	2.245(3)	−	2.227(2)

Bond angles/°

	2	**3**[a]	**4**
P(1)−Rh(1)−P(2)	96.97(12)	102.95(8)	92.96(7)
P(1)−Rh(1)−P(3)	160.58(13)	158.62(9)	165.07(7)
P(2)−Rh(1)−P(3)	102.38(12)	98.41(8)	100.80(7)
P(4)−Rh(2)−P(5)	100.02(12)	−	95.19(7)
P(4)−Rh(2)−P(6)	163.34(12)	−	106.44(8)
P(5)−Rh(2)−P(6)	96.48(12)	−	158.18(9)
Cl(1)−Rh(1)−Rh(2)	175.81(9)	178.02(6)	173.62(5)
Cl(2)−Rh(2)−Rh(1)	176.83(9)	−	91.88(5)

Torsion angles/°

	2	**3**[a]	**4**
P(1)−Rh(1)−Rh(2)−P(4)	19.44(13)	23.2	32.05(7)
P(2)−Rh(1)−Rh(2)−P(5)	22.55(12)	−32.5	30.13(7)
P(3)−Rh(1)−Rh(2)−P(6)	16.73(12)	−32.5	−27.14(8)

[a] Distances and angles of symmetry equivalent groups, denoted by −, are reported only once. Rh(2) = Rh(1A); P(4) = P(1A); P(5) = P(3A); P(6) = P(2A). [b] Rh(2)−Cl(2) is Rh(1)−Cl(2).

obtained from the hydrogenation reaction. X-ray structure determination reveals an octahedral coordination geometry about each rhodium center, with the chlorides ligated trans to the metal−metal bond and the tfepma ligands strapping the bimetallic core in a triply bridging motif. The coordination of the phosphite ligands about the rhodium centers exhibits a meridonal geometry with the P−Rh−P bond angles approaching 90°. The presence of two hydrides, although not located crystallographically, is implied by two open coordination sites in equatorial planes trans to P(2) and P(5). A strong trans influence is evidenced by the increased bond length of 2.303(3) Å for the Rh−P bond diametrically opposed to the hydride as compared to Rh−P bonds that are not (d_{avg}(Rh−P) = 2.240 Å). Additionally the P(1)−Rh(1)−P(3) angle of 160.58(13)° is indicative of the reduced steric requirements for the hydride as compared to the bulky bis(trifluorethoxy)phosphino unit of the tfepma ligand. The P(2)−Rh(1)−Rh(2)−P(5) dihedral angle of 22.55(12)° for the trans phosphite ligand is indicative of a syn disposition of the hydrides. Coordination of a chloride and a hydride to each rhodium center is consistent with the formulation of a valence symmetric $Rh_2^{II,II}$ core that results from the formal oxidative addition of hydrogen to the $Rh_2^{0,II}$ core of **1**. The Rh−Rh bond length of 2.7087(12) Å is typical of d^7−d^7 bimetallic systems.[35−37] The ^{1}H NMR spectrum of **2** in THF-d_8 concurs with the observed crystal structure. Two N−Me resonances are observed that integrate with a 2:1 ratio at 2.89 and 3.06 ppm, respectively, and a complicated hydride pattern, integrating as two protons, is centered at −9.77 ppm. The ^{31}P{^{1}H} NMR again is consistent with the observed solid-state structure, with two resonances observed in a 2:1 ratio at 136.76 and 131.40 ppm, respectively.

Concentrated solutions of **2** in CH_3CN left undisturbed deposit yellow blocks of **3**. The crystal structure of **3**, shown in Figure 2, reveals it to be an isomeric form of **2** with three bridging tfepma ligands spanning the core, two chlorides in axial positions trans to the metal−metal bond, and equatorially coordinated hydrides. As in **2**, the Rh−Rh bond of 2.7127(13) Å is well within the range of distances expected for a single metal−metal bond. The octahedral coordination geometry is maintained as defined by the P−Rh−P bond angles listed in Table 3. Unlike **2**, however, where both arms of one tfepma ligand are coordinated trans to the hydrides, the phosphite arms trans to the hydrides originate from two different tfepma ligands resulting in an anti presentation of the hydrides. The large trans influence of the hydrides[38] is again evidenced by the increased Rh−P bond length of 2.293(3) Å as compared to d_{avg}(Rh−P) = 2.25 Å for the other Rh−P bonds.

A third isomer, **4**, is also obtained from CH_2Cl_2/pentane washings set aside from the isolation of **2**. As shown by the crystal structure reproduced in Figure 2, one Rh^{II} center is coordinated by two chlorides and the other Rh^{II} center is coordinated by two hydrides. The chlorides and void spaces for the hydrides are disposed in an anti conformation about the bimetallic core. The coordination geometry about the rhodium center bonded to the hydrides is similar to that observed for both **2** and **3**, with increased lengths observed for Rh−P bonds

(35) Jenkins, J. A.; Ennett, J. P.; Cowie, M. *Organometallics* **1988**, *7*, 1845−1853.
(36) Cotton, F. A.; Eagle, C. T.; Price, A. C. *Inorg. Chem.* **1988**, *27*, 4362−4368.
(37) Cotton, F. A.; Dunbar, K. R.; Verbruggen, M. G. *J. Am. Chem. Soc.* **1987**, *109*, 5498−5506.
(38) Crabtree, R. H. *The Organometallic Chemistry of the Transition Metals*; Wiley: New York, 1994.

trans to hydride (see Table 3). Additionally, the P(5)−Rh(2)−P(6) bond angle of 158.18(9)° agrees well with those observed in **2** and **3**, where phosphite ligands are in a trans position to hydride. Although the same octahedral geometry is obtained for **4** as in **2** and **3**, the cis coordination of two hydrides and chlorides brings about some notable metric deviations. Trans ligation of Cl to P yields a d(Rh−P) = 2.1930(19) Å, which is markedly shorter than the mutually trans Rh(1)−P and Rh−P bonds on the metal center coordinated by the chlorides. This observation is consistent with the diminished trans influence of chloride versus phosphines.[39] The Rh−Rh bond length of 2.7657(8) Å and Rh−Cl_{ax} bond length of 2.5442(19) Å are significantly increased from the analogous bond lengths observed in **2** and **3**. These bond length increases are indicative of the presence of a strong σ-donating hydride in the axial position of Rh(2).

The results of nonlocal density functional theory show that complexes **2**, **3**, and **4** are nearly isoenergetic (ΔE = 470 cm^{-1}, see Table S12). Analytical frequency calculations were undertaken to assess the nature of the energy minima as determined by geometry optimization; zero point correction were made to the calculated energies of each of the ground-state molecules. Tables S13−S15 compare calculated bond lengths of the optimized structures of the dirhodium model complexes to the experimental metrics of the authentic compounds. For computed molecules, fluorine atoms act as surrogates for trifluoroethoxy groups on phosphorus of the tfepma ligands, and hydrides, not located crystallographically, were placed at idealized positions with an M−H bond length of 1.600 Å. Agreement between calculated and observed structures suggests that these simplifications are reasonable. Consistent with the prediction that **2** is less stable than **3**/**4** (see Table S11), solutions of **2** left to stand in the dark show the growth of new products in the ^{1}H NMR with time (∼24 h). This is evidenced by the appearance of N−Me resonances that are consistent with **3** and **4**.

Because conversion of **2** to **3** and **4** is slow, hydrogen elimination from freshly prepared solutions of the **2** may be examined without the complication by the participation of the other isomers. Solutions of **2** in THF-d_8 maintained in the dark showed no reaction upon exposure to HCl. ^{1}H NMR spectra obtained periodically over 1 week exhibited only the growth of resonances consistent with the aforementioned isomerization of **2** to **3** and **4**. The absence of an acid−base chemistry, which is not unusual in light of the well-known relative acidities of late transition metal hydrides,[40] discounts a pathway for H_2 production in which the metal-bound hydride reacts directly with a proton.

NMR experiments also establish that the hydrides are nonexchangeable, and that H_2 production does not occur by a bimolecular elimination reaction. Although **2** isomerizes slowly to **3** and **4**, an H_2 exchange reaction may be examined by monitoring the ratio of the integrated ^{1}H NMR resonances for the N−Me and hydrides of all isomers. We find that this ratio is essentially invariant for solutions of **2** in THF-d_8, under a D_2 atmosphere, changing from an initial value of 9:2 to 9:1.7 after 8 days. The observation of minor isotopic exchange, even after long periods of exposure of **2** to D_2, indicates that the hydrides do not rapidly dissociate from the bimetallic core.

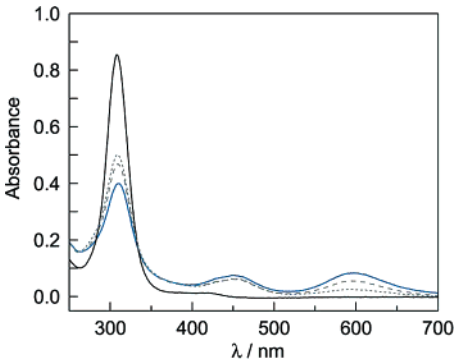

Figure 3. Changes in the electronic absorption spectrum during the photolysis (300 nm < λ_{exc} < 400 nm) of *syn*-$Rh_2^{II,II}(tfepma)_3H_2Cl_2$ (**2**) in THF. A blue photointermediate (—), produced within 30 s of irradiation, subsequently disappears over the course of 30 s (− − −) and 1 min (- - - -) after the excitation beam is blocked.

Photochemistry of 2. THF solutions of **2** immediately turn from yellow to blue upon irradiation into the dσ → dσ* absorption manifold (300 nm < λ_{exc} < 400 nm). As indicated by Figure 3, the color change results from the appearance of bands centered at 450 and 600 nm and the concomitant loss of the absorbance band at 308 nm over the course of the steady-state photolysis. As the 600 nm band disappears, the absorbance signatures of **1** are eventually recovered. ^{1}H NMR spectra of completely photolyzed solutions confirm that **1** is the final product. The conversion of the blue species to **1** is not markedly accelerated by UV or full spectrum radiation (λ_{exc} > 295 nm), as compared with solutions maintained in the dark after UV irradiation. Consequently, attempts to halt the photoreaction at the stage when the blue intermediate appeared were unsuccessful. These results suggest the overall reaction proceeds in a stepwise manner, beginning with a photoinduced process to give an initial blue photoproduct, which thermally rearranges to give **1**. Toepler pump experiments conducted on photolyzed solutions of **2** in THF-d_8 show the production of 0.94 equiv of a noncondensable gas, which burns over hot CuO. This result is consistent with the production of 1 equiv of H_2 per equiv of **2**:

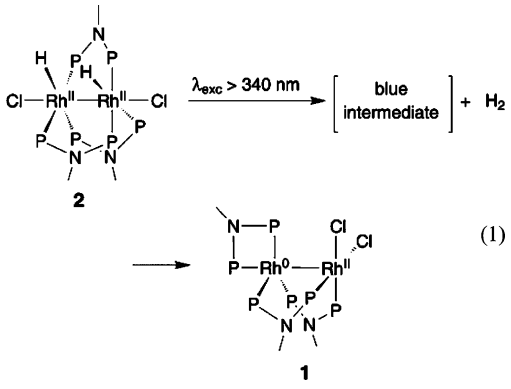

An independent ^{1}H NMR spectrum of the evolved gas shows only the sharp singlet of H_2 (4.52 ppm, CD_3CN); HD was not observed, thus ruling out the production of H_2 by an H-atom photoabstraction involving THF-d_8. Further insight into the H_2

(39) Collman, J. P.; Hegedus, L. S.; Norton, J. R.; Finke, R. G. *Principles and Applications of Organotransition Metal Chemistry*; University Science Books: Sausalito, CA, 1987.
(40) Labinger, J. A. Nucleophilic Reactivity of Transition Metal Hydrides. In *Transition Metal Hydrides*; Dedieu, A., Ed.; VCH publishers: New York, 1992; pp 361−379.

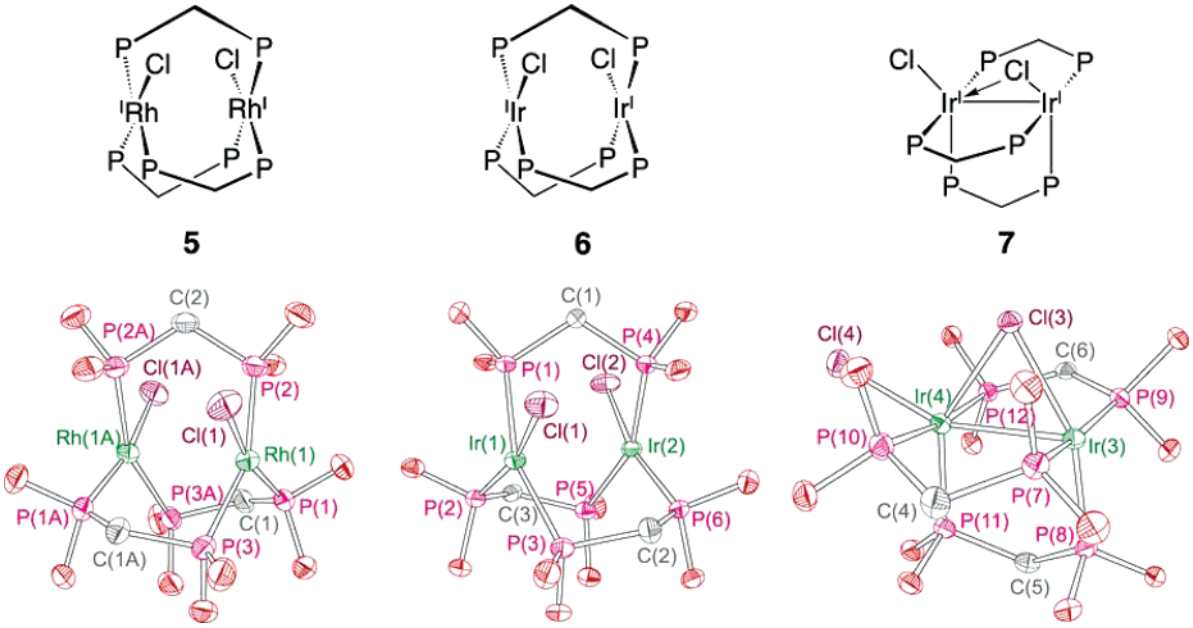

Figure 4. Tfepm complexes of dirhodium and diiridium: $Rh_2^{I,I}(tfepm)_3Cl_2$ (**5**), $Ir_2^{I,I}(tfepm)_3Cl_2$ (**6**), and $Ir_2^{I,I}(tfepm)_3(\mu\text{-}Cl)(Cl)$ (**7**). Thermal ellipsoids are drawn at the 50% probability level, and hydrogens and $-CH_2CF_3$ groups of the tfepm ligand have been omitted for clarity. Only atom numbers of pertinence to Table 4 are included. Full atom numbering scheme is presented in Supporting Information.

photoprocess comes from performing photolysis on equimolar mixtures of **2** and **2**-d_2 in THF-d_8; H_2 (>95%) and D_2 are predominantly obtained with HD produced in only minor yields (4.50 ppm, $^1J_{HD}$ = 43 Hz, CD_3CN). The absence of a statistical quantity of the isotopically scrambled HD supports a photoreaction in which hydrogen is produced by intramolecular reductive elimination. The minor occurrence of HD can be potentially attributed to one of the isomers of **2**, the photochemistry of which has not been explored at this point.

We next sought to identify the blue photoproduct of eq 1. The N−Me bridgehead of tfepma was replaced with a methylene unit, providing the tfepm ligand, $H_2C[P(OCH_2CF_3)_2]_2$. Treatment of saturated CH_2Cl_2 solutions of $[Rh^I(COD)Cl]_2$ with 3 equiv of tfepm provides the blue−purple compound, **5**, in good yield. An X-ray crystal structure of **5** (Figure 4) shows it to be a $ClRh^I\cdots Rh^ICl$ complex, where three phosphite ligands and a chloride assume an approximately square planar geometry about both rhodium centers. Deviation from a perfect square plane is slight, as indicated by the nearly orthogonal Cl−Rh−P and a P−Rh−P bond angles listed in Table 4. The Rh−P bond, trans to chloride, is slightly shorter (~0.1 Å) than those trans to another Rh−P bond; the Rh−Cl bond distances are similar to those observed in **2**−**4**. The Rh···Rh distance of 3.2780(4) Å is significantly elongated from that expected for a single metal−metal bond, but shorter than that for noninteracting metal centers. These observations are consistent with a stabilized metal−metal interaction engendered by configurational mixing of the filled dσ−dσ* and empty pσ−pσ* orbital manifolds; the metal−metal interaction resulting from this configuration interaction has been estimated to be on the order of 10−20 kcal/mol.[41]

The presence of an intense, low-energy band centered at 507 nm in the absorption spectrum of **5** (Figure 5) is a hallmark of the electronic structure of face-to-face $d^8\cdots d^8$ dimers. Simple electronic structure considerations lead to an assignment of a dσ* → pσ transition for the absorption profile,[42−46] which exhibits both the low energy and strong intensity that is

Table 4. Selected Crystallographic Bond Distances (Å) and Angles (°) for Complexes **5**, **6**, and **7**

Bond lengths/Å

	5[a]	**6**[b]	**7**[c]
M(1)−M(2)			2.7412(4)
M(1)−Cl(1)	2.3801(8)	2.4010(17)	2.4659(14)
M(2)−Cl(2)	−	2.3976(17)	2.4814(15)
M(2)−Cl(1)			2.5449(15)
M(1)−P(1)	2.1608(7)	2.2423(16)	2.2787(16)
M(1)−P(2)	2.2538(6)	2.1635(16)	2.1688(15)
M(1)−P(3)	2.2641(7)	2.2592(16)	2.3112(15)
M(2)−P(4)	−	2.2495(16)	2.3113(16)
M(2)−P(5)	−	2.2604(14)	2.1565(16)
M(2)−P(6)	−	2.1670(16)	2.3179(15)

Bond angles/°

	5	**6**	**7**
P(1)−M(1)−P(2)	94.46(3)	94.40(6)	95.39(6)
P(1)−M(1)−P(3)	100.44(3)	158.24(6)	167.63(6)
P(2)−M(1)−P(3)	158.80(3)	101.85(6)	93.91(6)
P(4)−M(2)−P(5)	−	157.72(5)	94.41(6)
P(4)−M(2)−P(6)	−	94.91(6)	173.11(6)
P(5)−M(2)−P(6)	−	101.62(6)	92.29(6)
Cl(1)−M(1)−M(2)	105.70(3)	106.25(4)	58.23(3)
Cl(2)−M(2)−M(1)	−	107.39(5)	156.49(4)

Torsion angles/°

	5	**6**	**7**
P(1)−M(1)−M(2)−P(4)	18.8	50.4	−0.4
P(2)−M(1)−M(2)−P(5)	−49.6	−16.1	−1.8
P(3)−M(1)−M(2)−P(6)	18.8	−15.9	−3.9
Cl(1)−M(1)−M(2)−Cl(2)	110.6	−107.2	−3.1

[a] Distances and angles of symmetry equivalent groups, denoted by the −, are reported only once for clarity. Atoms not within bonding distance are denoted by blank entries. M(1) = Rh(1), M(2) = Rh(1a), Cl(2) = Cl(2A), P(4) = P(3A), P(5) = P(2A), and P(6) = P(1A). [b] M = Ir. [c] M = Ir. The atom enumerations on the left correspond to a naming scheme of M(n) = M(n+2), Cl(n) = Cl(n+2), P(n) = P(n+6) in the thermal ellipsoid plot.

(41) Rice, S. F.; Miskowski, V. M.; Gray, H. B. *Inorg. Chem.* **1988**, *27*, 4704−4708.

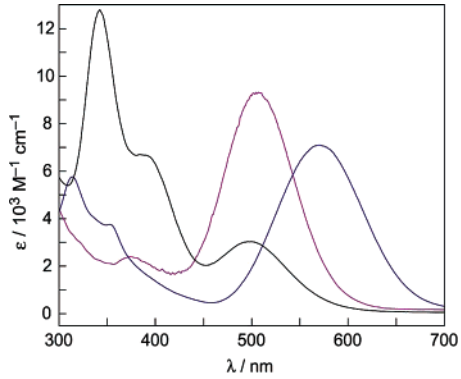

Figure 5. Electronic absorption spectra for complexes **5** (magenta line) and **6** (blue line) in toluene and **7** (black line) in Et_2O.

characteristic of such transitions. On the basis of these results, we believe that the blue intermediate in eq 1 is the valence symmetric, face-to-face $d^8\cdots d^8$ dimer, $Rh_2^{I,I}(tfepma)_3Cl_2$, which is the compound expected to be produced directly upon the reductive elimination of H_2 from **2**.

The face-to-face $d^8\cdots d^8$ dimer of iridium is also afforded by a reaction similar to that employed for the preparation of **5**. In this case, two chemically distinct molecules, **6** and **7**, are present in the asymmetric unit. **6** can be uniquely prepared and crystallized (see Supporting Information). It is structurally similar to **5** and is entirely consistent with the assignment of a valence symmetric $Ir_2^{I,I}$ core (see Figure 4 and Table 4). The metal−metal distance in **6** of 3.2641(4) Å is slightly shorter (by ∼0.01 Å) than that observed for **5** but is still outside that expected for a formal single bond. The shorter metal−metal distance is consistent with a larger configuration interaction arising from greater overlap of 5d orbitals. Moreover, this greater orbital overlap leads to larger $d\sigma-d\sigma^*$ and $p\sigma-p\sigma^*$ splittings, which in turn are manifested in an attenuated energy gap for the $d\sigma^* \rightarrow p\sigma$ transition as compared to **5**, accounting for the red-shift shown in Figure 5 for the low-energy absorption of **6**. The other molecule in the asymmetric unit cell, **7**, is a fascinating complex with a chloride ion folded over into a bridging position between the diiridium centers. The crystal structure of the compound shown in Figure 4 is a snapshot of the intermetal chloride migration that takes the symmetric $ClM^I\cdots M^ICl$ core to an internally disproportionated $M^0-M^{II}Cl_2$ core. An asymmetry in the Ir−Cl(bridge) bond lengths, d(Ir(3)−Cl(3)) = 2.4659(14) Å and d(Ir(4)−Cl(3)) = 2.5449(15) Å, suggests that a chloride lone pair participates in a dative Cl → Ir bonding interaction. A significant metal−metal interaction is also indicated by an Ir−Ir distance of 2.7412(4) Å, which is well within the range expected for a single metal−metal bond. The bridging tfepm ligands are nearly eclipsed, with an average P−Ir−Ir−P dihedral angle of 2°. The terminal chloride cants significantly from the plane defined by the phosphorus atoms of the tfepm ligands as signified by a Cl−Ir−P bond angle of 114.61(6)°, engendering an overall trigonal bipyramidal geometry about Ir(4).

Compound **7** indicates that bimetallic cores ligated by tfepm are on the razor's edge of mixed valency. The reaction chemistry of **5** with σ-donor ligands confirms this contention. Treatment of **5** with 1 equiv of *tert*-butylisonitrile leads to rapid and quantitative conversion to **8**:

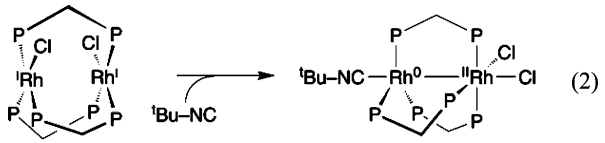

(2)

The low-energy absorption band of **5** is lost, and an electronic absorption spectrum of a complex containing a $Rh_2^{0,II}$ core is obtained (Figure 5).[47] An X-ray crystal structure of **8** (Figure S9) reveals the familiar ligand environment that we have observed previously for metal−metal bonded $Rh_2^{0,II}$ cores spanned by three diphosphazane ligands. The Rh^{II} center assumes an octahedral coordination sphere with the P atoms of the tfepm ligands assuming a *mer* configuration. The neighboring Rh^0 center and chlorides complete the primary coordination sphere. The Rh^0 center is trigonal bipyramidal, with three P atoms of the tfepm occupying the equatorial plane and the isonitrile and Rh^{II} center occupying the axial coordination sites. The crystal structure of **8**, however, is notable from typical $Rh_2^{0,II}$ diphosphazane complexes in one regard: an alteration in bond lengths of the ligand backbone is absent. The average P−C bond lengths proximal to the Rh^0 and Rh^{II} centers are identical within error, and are ∼0.15 Å longer than the P−N bonds observed in the crystal structure of congener **9** (Figure S10), $Rh_2^{0,II}(dfpma)_3Cl_2(CN^tBu)$, in which tfepm is replaced with the A−D−A stereoelectronic motif of dfpma. For the latter, the average P−N bond length proximal to Rh^{II} is ∼0.03 Å shorter than that of the P−N bonds proximal to Rh^0. This bond alteration is believed to play a pivotal role in enforcing two-electron mixed valency (vide infra). Indeed, in no case has a $Rh_2^{I,I}$ center been isolated when coordinated by three A−D−A ligands. Only when the capacity for stereoelectronic asymmetry is absent in the ligand backbone, as in the case of tfepm, is the valence symmetric bimetallic core realized as an isolable product.

Discussion

The formal oxidation states for binuclear cores comprised of group 9 metals may be controlled by modifying the stereoelectronic properties of a bidentate phosphine ligand, as outlined in Figure 6. Ligands possessing an A−D−A motif stabilize M^n-M^{n+2} cores. Conversely, a wealth of dirhodium chemistry shows that a valence symmetric $M^{n+1}\cdots M^{n+1}$ core is obtained for "electronically neutral" ligands, such as bridging phosphines.[46,48−52] Complexes at these formal oxidation state limits may be obtained by tuning the electron-donating properties of the bridgehead and the electron-withdrawing properties of the phosphine (middle panel), thus allowing the relevant intermediates of the H_2 photocycle shown in Figure 1 to be unveiled.

(42) Mann, K. R.; Gordon, J. G., II; Gray, H. B. *J. Am. Chem. Soc.* **1975**, *97*, 3553−3555.
(43) Rice, S. F.; Gray, H. B. *J. Am. Chem. Soc.* **1981**, *103*, 1593−1595.
(44) Fordyce, W. A.; Brummer, J. G.; Crosby, G. A. *J. Am. Chem. Soc.* **1981**, *103*, 7061−7064.
(45) Balch, A. L. *J. Am. Chem. Soc.* **1976**, *98*, 8049−8054.
(46) Balch, A. L.; Tulyathan, B. *Inorg. Chem.* **1977**, *16*, 2840−2845.
(47) Kadis, J.; Shin, Y. G.; Dulebohn, J. I.; Ward, D. L.; Nocera, D. G. *Inorg. Chem.* **1996**, *35*, 811−817.
(48) Mague, J. T.; Mitchener, J. P. *Inorg. Chem.* **1969**, *8*, 119−125.
(49) Sanger, A. R. *J. Chem. Soc., Chem. Commun.* **1975**, 893−894.
(50) Kubiak, C. P.; Eisenberg, R. *J. Am. Chem. Soc.* **1977**, *99*, 6129−6131.
(51) Cowie, M.; Mague, J. T.; Sanger, R. A. *J. Am. Chem. Soc.* **1978**, *100*, 3628−3629.
(52) Puddephatt, R. *J. Chem. Soc. Rev.* **1983**, *12*, 99−127.

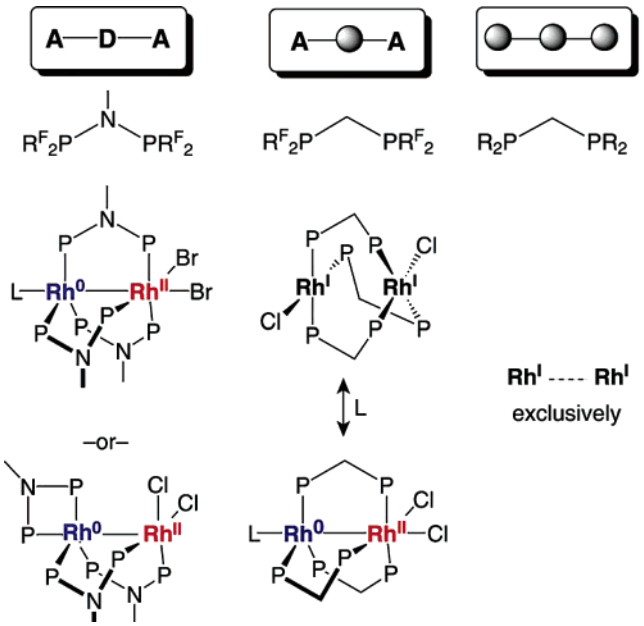

Figure 6. Schematic that summarizes the relation between the electronic structure of a bridging bidentate ligand and the formal oxidation state of a dirhodium binuclear core.

Expected HX addition products to a $Rh_2^{0,0}$ core are isolable when the stereoelectronic strength of the phosphine, as defined by Tolman,[18] is attenuated from $-PF_2$ to $-P(OCH_2CF_3)_2$. All isomers are obtained for arranging two halides and two hydrides about a dirhodium core spanned by three bidentate ligands. The slow interconversion of **2** to **3** and **4** on the time scale of the observed photochemistry allows for a detailed study of H_2 photoelimination from a $Rh_2^{II,II}(H)_2(Cl)_2$ core. Excitation of **2** leads to the prompt production of an equivalent of H_2 by an intramolecular photoinduced reductive elimination to yield a blue complex with an absorption spectrum (blue trace, Figure 5) that is notably similar to that observed for a nonisolable intermediate of the authentic photocycle (blue trace, Figure 1). In our initial report of the H_2 photocycle,[16] the blue compound was tentatively proposed to be a tetranuclear rhodium species based on observations of dirhodium isonitrile chemistry. Oxidation of $Rh_2^{I,I}$ cores bridged by bidentate isonitriles yields $[Rh^IRh^{II}Rh^{II}Rh^I]^{6+}$ tetramers, which are blue.[53] However, the tfepm chemistry reported here clearly shows this not to be the case. Blue $ClM^I\cdots M^ICl$ (M = Rh and Ir) compounds **5** and **6** can be isolated and characterized when the N−Me donor of the tfepma bridgehead is replaced by the methylene unit of tfepm. The blue color of **5**/**6** is characteristic of a transition resulting from a $d\sigma^* \rightarrow p\sigma$ transition of a face-to-face $d^8\cdots d^8$ dimer. We note that the blue compounds observed in the photocycle of Figure 1 and the H_2 photoelimination chemistry of **2** ($Rh_2^{I,I}$ cores bridged by PNP = dfpma and tfepma ligands, respectively) possesses a low-energy maximum that is red-shifted from that of **5** (a $Rh_2^{I,I}$ core tfepm bridge). The sensitivity of the $d\sigma^* \rightarrow p\sigma$ transition energy to metal−metal distance most likely explains this variation in absorption maxima of the different blue compounds bridged by different bidentate fluorophosphine ligands. The increased $P-CH_2-P$ bond length of tfepm in **8** as compared to P−N(Me)−P of dfpma in **9** (by ~0.15 Å) manifests itself in an increased M−M bond distance. A similar increase in M···M distance in **5** would serve to increase the $d\sigma^* \rightarrow p\sigma$ transition energy of this complex as compared to $ClRh^I\cdots Rh^ICl$ cores bridged by diphosphazane ligands. In light of the structural sensitivity of the absorption maximum to metal−metal distance, we attribute the blue species observed in HX photocatalysis as a valence symmetric $Rh_2^{I,I}(dfpma)_3Cl_2$ complex.

A face-to-face $Rh_2^{I,I}(PNP)_3Cl_2$ (PNP = dfpma and tfepma) complex is expected for direct photoinduced elimination of H_2 from **2**. Mechanistic insight for this photoelimination is provided by experimental and computational studies of diiridium tfepma hydride and hydrido−halide complexes. In these systems, both hydrogen addition and elimination are mediated by a bridging hydride.[12,13]

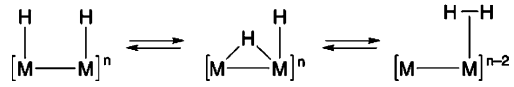

(3)

The bridging hydride intermediate is akin to bimolecular binuclear elimination pathways,[54−56] and it is also consistent with the observations of Stanley and collaborators,[57−61] who have shown that H_2 is readily activated by dirhodium tetraphosphine complexes. In these systems, initial oxidative addition of H_2 to a single center of a bimetallic $Rh_2^{I,I}$ core initially affords a two-electron mixed-valence $Rh_2^{I,III}$ dihydride that rearranges to a $Rh_2^{II,II}$ center, presumably through a bridging hydride intermediate. Owing to the prevalence of a bridging hydride in managing H_2 at the bimetallic cores of diiridium tfepma chemistry and related dirhodium tetraphosphine complexes, we surmise that a μ-H intermediate also plays a role in the photoelimination of H_2 from **2**.

The $ClRh^I\cdots Rh^ICl$ dimers convert to $Rh^0-Rh^{II}Cl_2$ mixed-valence cores with facility, especially when the bridging ligand is a diphosphazane. For dirhodium cores bridged by tfepma, the coordination mode of **1** is obtained, whereas cores bridged by dfpma yield **9**. This observation is consistent with computational and experimental studies that show sterically bulky adjuncts on phosphorus serve to increase the tendency of these ligands to adopt chelating binding modes.[32,33] This contention is supported by the chemistry of tfepm, which accommodates $Rh_2^{I,I}$ and $Rh_2^{0,II}$ cores. In the absence of the A−D−A stereoelectronic impetus, an external ligand is required to convert the valence symmetric core of **5** to the valence asymmetric core of **8**. In view of **7**, we believe that the $ClRh^I\cdots Rh^ICl$ primary photoproduct of the H_2 photocycle in Figure 1 and H_2 photochemistry of **2** converts to their respective $Rh^0-Rh^{II}Cl_2$ via a μ-Cl intermediate.

(53) Sigal, I. S.; Mann, K. R.; Gray H. B. *J. Am. Chem. Soc.* **1980**, *102*, 7252−7256.
(54) Norton, J. R. *Acc. Chem. Res.* **1979**, *12*, 139−145.
(55) Martin, B. D.; Warner, K. E.; Norton, J. E. *J. Am. Chem. Soc.* **1986**, *108*, 33−39.
(56) Kristjánsdóttir, S. S.; Norton, J. A. In *Transition Metal Hydrides*; Dedieu, A., Ed.; VCH: New York, 1992; Chapter 9, pp 309−360.
(57) Broussard, M. E.; Juma, B.; Train, S. G.; Peng, W.-J.; Laneman, S. A.; Stanley, G. G. *Science* **1993**, *260*, 1784−1788.
(58) Carter, R. D.; Howell, D. K.; Peng, W.-J.; Train, S. G.; Treleaven, W. D.; Stanley, G. G. *Angew. Chem., Int. Ed. Engl.* **1996**, *35*, 2253−2256.
(59) Peng, W.-J.; Train, S. G.; Howell, D. K.; Fronczek, F. R.; Stanley, G. S. *Chem. Commun.* **1996**, 2607−2608.
(60) Laneman, S. A.; Fronczek, F. R.; Stanley, G. G. *J. Am. Chem. Soc.* **1988**, *110*, 5585−5586.
(61) Stanley, G. In *Catalysis by Di- and Polynuclear Metal Cluster Complexes*; Adams, R. D., Cotton, F. A., Eds.; Wiley-VCH: New York, 1998; pp 345−372.

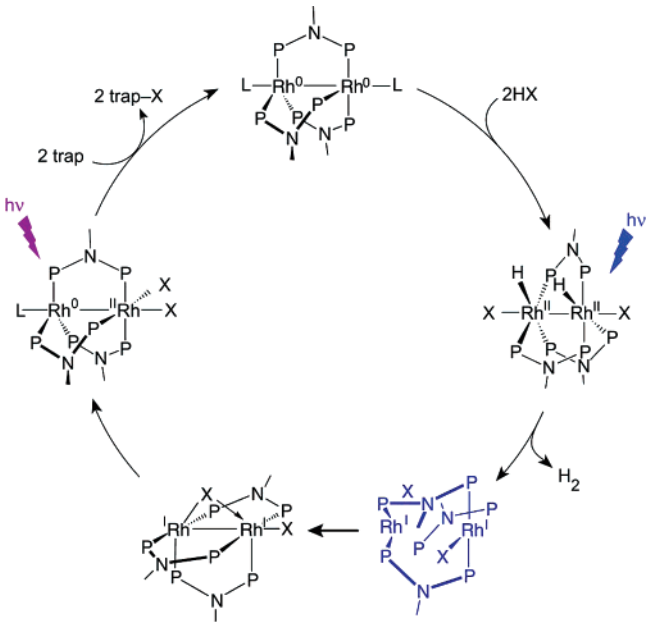

Figure 7. The complete photocycle for H_2 generation by a Rh_2 dfpma photocatalyst. The proposed intermediates of the cycle are based on the chemistry of dirhodium and diiridium tfepma and tfepm synthetic analogues.

On the basis of the foregoing chemistry of tfepma and tfepm dirhodium analogues, we propose that Rh_2 dfpma produces H_2 from HX by the photoprocess shown in Figure 7. HX addition to the $Rh_2^{0,0}$ core produces the $Rh_2^{II,II}$ dihydride−dihalide, which photoeliminates 1 equiv of H_2 and generates the blue $XRh^I\cdots Rh^IX$ (X = Cl, Br) complex. This valence symmetric, primary photoproduct, is unstable with respect to internal disproportionation to the $Rh^0-Rh^{II}X_2$ core; the disproportionation proceeds by folding a terminal halide into the bridging position of the dirhodium core. Photoexcitation of the $Rh^0-Rh^{II}X_2$ leads to halogen atom elimination and regeneration of the coordinatively unsaturated Rh^0-Rh^0 complex, for reentry into the photocycle.

As we have previously discussed, the overall photoefficiency for H_2 production by the photocycle in Figure 7 is ~1%, commensurate with that observed for Rh−X bond photoactivation.[16] Whereas H_2 photoelimination from the $Rh_2^{II,II}H_2Cl_2$ is efficient, as deduced from the photochemistry of **2**, the photoconversion of $Rh_2^{0,II}(dfpma)_3X_2L$ to $Rh_2^{0,0}(dfpma)_3L_2$ has been independently measured to proceed with a quantum efficiency of ~1%,[14,15] indicating that the activation of the Rh−X bond is the critical determinant to overall photocatalytic activity. Accordingly, the work described herein establishes that the issue of H_2 photoefficiency is not directly related to the primary photoprocess of H_2 photoelimination from the dihydride but rather is equated to halogen atom elimination from the bimetallic core. Toward this end, current studies aimed at achieving higher H_2 yields target strategies to promote the efficient multielectron photoactivation of M−X bonds.

Acknowledgment. This work was supported by the National Science Foundation (CHE-0450058).

Supporting Information Available: Full reference for the Gaussian 98 computational package, Cartesian coordinates for the optimized geometries obtained from Gaussian calculations, calculated energies, thermal ellipsoid plots, tables of crystal data, atomic coordinates, bond lengths and angles, anisotropic thermal parameters, and hydrogen coordinates for complexes **1**−**9**. This material is available free of charge via the Internet at http://pubs.acs.org.

JA054371X